IJRCS

International Journal of Robotics and Control Systems
Vol. 5, No. 1, 2025, pp. 1-21
ISSN 2775-2658
http://pubs2.ascee.org/index.php/ijrcs

ASCEE

Comparative Analysis of Sensor Fusion for Angle Estimation Using Kalman and Complementary Filters

Phichitphon Chotikunnan [a,1], Wanida Khotakham [a,2], Alfian Ma'arif [b,3], Anuchit Nirapai [a,4,*], Kanyanat Javana [c,5], Pawichaya Pisa [c,6], Phanassanun Thajai [c,7], Supachai Keawkao [c,8], Kittipan Roongprasert [a,9], Rawiphon Chotikunnan [a,10], Pariwat Imura [a,11], Nuntachai Thongpance [a,12]

[a] College of Biomedical Engineering, Rangsit University, Pathum Thani 12000, Thailand
[b] Universitas Ahmad Dahlan, Yogyakarta 55191, Indonesia
[c] Triamudom Suksa Nomklao Uttaradit School, Mueang District, Uttaradit 53000, Thailand
[1] phichitphon.c@rsu.ac.th; [2] wanida.k@rsu.ac.th; [3] alfianmaarif@ee.uad.ac.id; [4] anuchit.ni@rsu.ac.th;
[5] kanyanat@tunu.ac.th; [6] pawichayapisav@tunu.ac.th; [7] phanassanun@tunu.ac.th; [8] supachai@tunu.ac.th;
[9] kittipan.r@rsu.ac.th; [10] rawiphon.c@rsu.ac.th; [11] pariwat.i@rsu.ac.th; [12] nuntachai.t@rsu.ac.th
* Corresponding Author

ARTICLE INFO

Article history
Received October 05, 2024
Revised November 07, 2024
Accepted November 28, 2024

Keywords
IMU6050;
Kalman Filter;
Complementary Filter;
Sensor Fusion

ABSTRACT

In engineering, especially for robots, navigation, and biomedical uses, accurate angle estimation is absolutely crucial. Using data from the IMU6050 sensor, which combines accelerometer and gyroscope readings, this work contrasts two sensor fusion methods: the Kalman filter and the complementary filter. The aim of the research is to find the most efficient filtering method for preserving accuracy and resilience throughout several motion contexts, including low-noise (standard rotation) and high-noise (external disturbances). With an eye toward improving sensor accuracy in dynamic applications, the study contribution is a thorough investigation of filter performance under different noise levels. MATLAB quantified estimate accuracy using key metrics like root mean square error (RMSE) and mean absolute error (MAE). Under controlled noise levels, our approach included methodical error analysis of both filters. Results show that, especially under low-noise conditions, the Kalman filter beats the complementary filter in terms of lower MAE and RMSE; it also shows adaptability and robustness in high-noise environments with much fewer errors than accelerometer-only and complementary filter outputs. These results show the relevance of the Kalman filter in practical settings like robotic control, motion tracking, and possible biomedical equipment, including patient positioning systems and wheelchairs with balance control. Future studies might investigate the implementation of the Kalman filter in sophisticated systems requiring accuracy, such as telemedicine robots or autonomous navigation. This work develops sensor fusion techniques and offers understanding of consistent sensor data processing in several operating environments.

1. Introduction

Precise angle estimation is crucial in engineering domains including robotics, aircraft, and navigation systems, where accurate orientation is vital for operational dependability and control [1], [2]. Accurate angle estimation is essential in biomedical applications, particularly surgical robots for

precise motions and autonomous drones for stability maintenance [3]. Traditional methods that depend either on gyroscopes or accelerometers are often susceptible to noise, drift, and external interferences, resulting in significant estimate inaccuracies [4]-[6]. Inertial Measurement Units (IMUs), which combine accelerometers and gyroscopes, enhance angle estimation precision; nonetheless, the successful fusion of data from many sensors continues to pose challenges for consistent and accurate orientation monitoring [7]-[9]. To tackle these issues, sensor fusion methods, including the Kalman filter and complementary filter, are extensively used in angle estimation applications [10]-[12]. The Kalman Filter is distinguished by its capacity to handle noisy input and adapt dynamically in real-time via continuous updates, rendering it very useful in applications including autonomous navigation, state prediction, and control systems for robots and drones [13]-[17]. Conversely, the complementary filter offers a more straightforward and computationally effective method by amalgamating high-frequency gyroscope data with low-frequency accelerometer data, yielding reliable orientation estimations for applications that value real-time performance [18]-[21]. Nonetheless, advanced Kalman filter models, particularly those employing Multiple Model (MM) filters, demonstrate enhanced reliability in intricate and noisy environments; yet, difficulties remain in adapting these filters to swift variations in dynamic systems [22]-[24].

Notwithstanding their efficacy, a thorough evaluation of these filters under diverse noise circumstances is still constrained. Although previous research has investigated their applicability in areas such as drone navigation, robotic tracking, and wearable devices [25]-[31], there is an absence of systematic assessment contrasting their performance in low-noise (standard rotations) and high-noise (disturbance) conditions. Advanced iterations of the Kalman Filter, such as the Extended Kalman Filter (EKF) and Unscented Kalman Filter (UKF), have shown resilience in managing dynamic situations and superiority in intricate contexts [32]-[39]. Nonetheless, the efficacy of the complementary filter may diminish considerably in dynamic or high-noise environments, especially where swift environmental alterations transpire, as it lacks the robust adaptability exhibited by advanced Kalman filter variants, which are more appropriate for conditions characterized by fluctuations and sensor uncertainties [34]-[36].

This work seeks to address the research gap by assessing the efficacy of the Kalman Filter and Complementary Filter using data from the IMU6050 sensor, which amalgamates accelerometer and gyroscope measurements [40]-[42]. Experiments are performed under diverse motion situations, including conventional rotations and produced disturbances, to identify the most precise and resilient filtering strategy for angle estimation. The research utilizes performance indicators, including mean absolute error (MAE) and root mean square error (RMSE), to assess the efficacy of each filter at various noise levels [43]-[45]. Furthermore, the Exogenous Kalman Filter (XKF) and hybrid neural network methods, which involve the combination of LSTM neural networks with Kalman filters, have also demonstrated potential in specialized contexts. These methods provide robustness in applications that necessitate state estimation under ambiguous conditions [46], [47]. The filtering accuracy and adaptability in dynamic settings, such as self-balancing and other robotics applications, have been further enhanced by techniques such as the dual augmented Kalman filter and reinforcement learning-integrated Kalman filtering [48], [49].

This study provides two main contributions. First, it provides empirical analysis of the strengths and constraints of several filters in diverse motion environments, thereby guiding the choice of the most appropriate filters for certain purposes [50]-[52]. Second, it shows how in dynamic settings adaptive filtering improves sensor fusion accuracy. These results should help to build strong orientation tracking systems in sectors including autonomous systems, biomedical devices, and advanced robotic control systems [53]-[57] that call for accuracy and adaptability.

2. Method

The method used in this study is made up of five main parts. First, a Kalman Filter method for estimating angle is created using information from the MPU6050 sensor, which records readings from both the gyroscope and the accelerometer. Two important parameters, Q (process noise

covariance) and *R* (measurement noise covariance), are changed dynamically in reaction to changes in sensor data to improve the accuracy and stability of estimation. The second part goes into detail about how to use the gyroscope and accelerometer data from the MPU6050 sensor, including how it is set up and the equations needed to estimate angles. This sets the stage for the Kalman and complementary filter analysis that follows. In the third step, a complementary filter is used to combine data from the gyroscope and accelerometer. This lowers the drift of the gyroscope and lowers the noise from the accelerometer. Equations that explain the process of data fusion show how the complementary filter helps make angle accuracy better. In the fourth step, a one-dimensional Kalman filter model is made just for estimating angles. This includes creating equations for time update (prediction) and measurement update (correction) to make sure the filter stays accurate as sensor data changes. Finally, the fifth step is all about finding the best values for *Q* and *R* in the Kalman filter. Here, *Q* and *R* are drawn from 20 sets of data, which lets the filter keep getting better by recalibration. Adjusting *Q* and *R* in this way makes it possible to get accurate and reliable angle estimates in a wide range of situations, which makes the filter useful in changing settings.

2.1. Algorithm Design of Kalman Filter for Angle Estimation in MPU 6050 Sensor System

The Kalman Filter algorithm for angle estimation, as depicted in Fig. 1, is intended to improve accuracy by perpetually updating two critical parameters: measurement noise covariance (*R*) and processing noise covariance (*Q*).

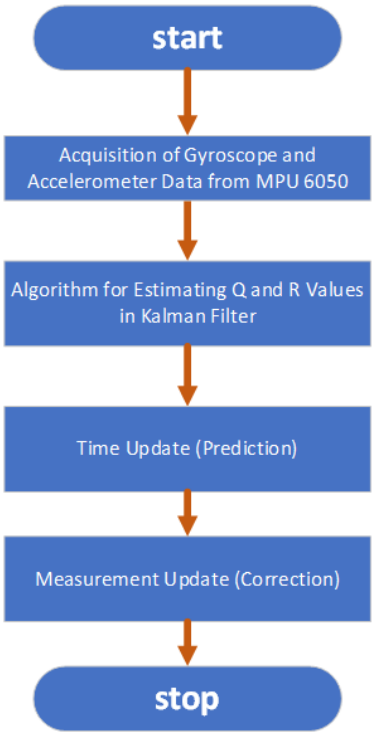

Fig. 1. Block diagram of the kalman filter algorithm

At first, *Q* and *R* are given numbers that are close to zero because giving them absolute zero would not work. The gyroscope and accelerometer's initial values are set to zero to make sure the device is stable. The 13-millisecond data acquisition frequency is meant to combine processing speed with timely updates. There are two separate parts to the Kalman filter: time update (prediction) and measurement update (correction). The Time Update guesses the current state based on the last state, and the Measurement Update improves this guess by using real-time sensor data from the MPU6050 sensor, which collects both gyroscopic and accelerometric data. For this study, rubber hammer impacts are used to create a simulated vibration environment that is meant to mimic the conditions of systems that are sensitive to vibrations, such as balancing robots and setups that are placed on vehicles. The goal of these tests is to see how well changing *Q* and *R* dynamically works compared

to using static values. This will improve the filter's ability to change and work well in changing environments. More mathematics information is given in Section 2.4.

2.2. Application of Gyroscope and Accelerometer: A Case Study of MPU6050

This study has selected the MPU6050 sensor, a 6 Degrees of Freedom (6DOF) Inertial Measurement Unit (IMU), for its cost-effectiveness and the incorporation of two critical sensors, a gyroscope and an accelerometer, in a single chip (see Fig. 2). This integration facilitates the synchronization of measurements and simplifies the calibration procedure. The MPU6050 is a critical component of a variety of engineering applications, such as balance robots and unmanned aerial vehicles (UAVs), as it provides essential data for motion and rotation.

Fig. 2. MPU6050

The incorporated Digital Motion Processor (DMP) of the MPU6050 sensor enables rapid data processing by measuring rotational and acceleration parameters across three axes. The I2C protocol facilitates communication, rendering the sensor compatible with a diverse array of programming tools. The MPU6050 facilitates the transmission of high-resolution data by incorporating a 16-bit analog-to-digital converter (ADC). The gyroscope is calibrated to measure up to±500 degrees per second, while the accelerometer is calibrated to capture measurements up to±4 g. These limits have been chosen for applications in which rotation velocities are less than 500 degrees per second and acceleration forces do not exceed 4 g.

The gyroscope's angular velocity (ω_{gyro}) is determined by applying the method in (1), with a measurement range of 500 degrees per second. In this context, the raw output of the gyroscope is denoted by LSB_{read}, the baseline measurement is $LSB_{Zero\ rotation\ value}$ when the device is stationary, and the typical sensitivity is a constant provided by the manufacturer.

$$\omega_{gyro} = \frac{LSB_{read} - LSB_{Zero\ rotation\ value}}{Nominal\ sensitivity} \tag{1}$$

For the accelerometer, angle estimation relies on Earth's gravity. The angle (θ) is determined based on the raw sensor data, as shown in (2). Similar to the gyroscope, LSB_{read} represents the raw output, $LSB_{Zero\ rotation\ value}$ is the baseline when stationary, and Nominal sensitivity converts the data into a physical quantity,

$$\theta_{Accele\ I} = arctan\left(\frac{LSB_{read} - LSB_{Zero\ rotation\ value}}{Nominal\ sensitivity}\right) \tag{2}$$

Under certain conditions, the angle θ_{Accele} can be refined by incorporating data from the Z-axis to account for additional directional forces, as shown in (3). This adjusted equation improves angle estimation accuracy by considering *X*, *Y*, and *Z* axis data.

$$\theta_{Accele\ II} = arctan\left(\left(\frac{LSB_{read} - LSB_{Zero\ rotation\ value}}{Nominal\ sensitivity}\right)\Big/\left(\frac{LSB_{read\ Z} - LSB_{Zero\ rotation\ value\ Z}}{Nominal\ sensitivity\ Z}\right)\right) \quad (3)$$

The concept of angular output from the accelerometer in relation to gravitational forces is illustrated in Fig. 3. This configuration enables the MPU6050 to detect and adjust to disturbances, rendering it well-suited for environments with vibration or minor impacts, such as those that are replicated by applying force to the testing surface to simulate real-world scenarios. The selection of the MPU6050 also demonstrates the necessity for a sensor that can generate consistent and dependable data within the constraints of low-cost systems, despite the potential for signal latency to be a limiting factor in comparison to analog sensors.

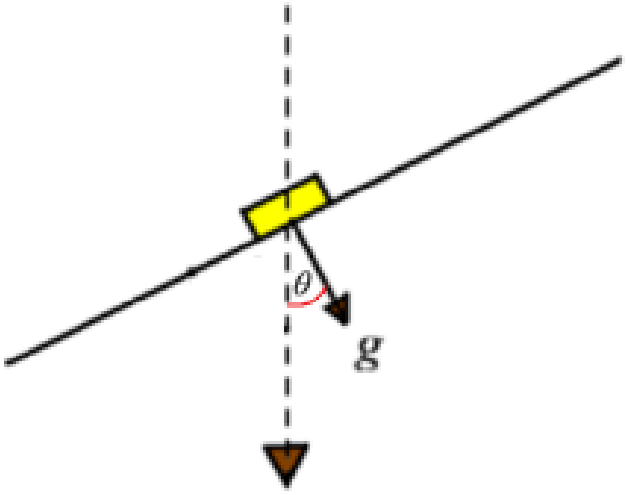

Fig. 3. Output of angular

2.3. Complementary Filter

The integration of data from devices with varying frequency characteristics produces a complementary filter that improves measurement precision [12]. This method, commonly employed in systems with dual input types, transmits high-frequency noise through a low-pass filter while utilizing low-frequency data, resulting in a process analogous to Wiener filtering. It effectively combines data from an accelerometer and a gyroscope, employing a complimentary filter to mitigate the limitations of each sensor while enhancing their advantages. This filter was selected because to its computational simplicity compared to more intricate filtering methods, while yet providing effective performance. Its uncomplicated design, necessitating only two configurable parameters, renders it optimal for fundamental angle estimation applications. The complementary filter is especially appropriate for embedded systems that prioritize real-time performance and precision due to its straightforward implementation and minimum computational resource requirements. The gyroscope delivers precise short-term rotational speed information but is prone to drift over time, whereas the accelerometer gives consistent long-term tilt measurements but is susceptible to short-term disturbances. By reducing the gyroscope's high-frequency noise and boosting the accelerometer's low-frequency stability, the complementary filter brings the two inputs together. This makes angle measurements accurate and reliable. The filter produces the outcome that is indicated in (4).

$$\gamma_k = \rho\alpha_{k-1} + \sigma\beta_{k-1} + \varepsilon_{k-1} \quad (4)$$

These coefficients, ρ and σ, represent the proportional weights assigned to the input of each sensor in this model. The noise component, denoted by the symbol ε_k, is frequently assumed to be zero in this context. The parameter dt is a minuscule constant of 0.013 seconds that specifies the time step. It is chosen to be consistent with the system's computational constraints and the frequency of data collection of the sensor. The Arduino Uno, which operates via RS232 and has restricted

processing capabilities, is guaranteed to adhere to the computational limitations of data collection and processing during this time phase. In order to obtain an appropriate balance between responsiveness and stability for this application, the parameters were manually adjusted to ρ = 0.9 and σ = 0.1. The computed values for α_k and β_k are presented in (5) and (6).

$$\alpha_k = (\gamma_{k-1} + (dt \times \omega_{gyro})) \tag{5}$$

$$\beta_k = \theta_{Accele} \tag{6}$$

The complementary filter's design achieves a balance between the accelerometer's long-term stability and the gyroscope's short-term precision, making it an appropriate choice for applications that require accurate angle estimates. This configuration is highly advantageous in practical applications that have limited computational capabilities, such as fundamental motion-tracking systems and balancing robotics. The block diagram of the complementary filter system is illustrated in Fig. 4.

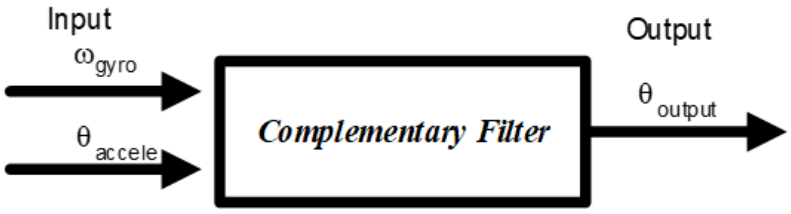

Fig. 4. Block diagram of complementary filter

2.4. Kalman filter

The Kalman filter [53] is a potent algorithm that is employed to estimate the state of dynamic systems by processing sequential data that is collected over time. It employs two fundamental processes, Time Update (Prediction) and Measurement Update (Correction), to progressively refine state estimates while operating in a discrete-time framework. The state variable at any given time, t_k , is represented as x_k, with the time steps designated as $t_0, t_1, t_2, \ldots, t_k$, where k indicates the iteration step. The forthcoming state is predicted by the state transition model in (7), which provides an evolving estimate with each step, based on the current state and control inputs.

$$x_k = Ax_{k-1} + Bu_{k-1} + w_{k-1} \tag{7}$$

For a two-dimensional state variable model, (8) is used.

$$\begin{bmatrix}\theta_k \\ \omega_k\end{bmatrix} = \begin{bmatrix}1 & 0 \\ 0 & 0\end{bmatrix}\begin{bmatrix}\theta_{k-1} \\ \omega_{k-1}\end{bmatrix} + \begin{bmatrix}\delta t \\ 1\end{bmatrix}u_{k-1} + \begin{bmatrix}0 \\ 1\end{bmatrix}w_{k-1} \tag{8}$$

Here, w_{k-1} represents the process noise, assumed to be a Gaussian random variable with zero mean, as expressed by (9) and variance Q_w, as depicted in (10). This assumption is essential for the Kalman filter's optimal performance in minimizing the estimation error. The process noise is further described as follows,

$$\mu_{w_k} = E[w_k] = 0 \tag{9}$$

$$Q_w = E[w_k w_k^T] = E[w_k w_j] = \begin{cases} Q_w \ , for \ k = j \\ 0 \ , \ for \ k \neq j \end{cases} \tag{10}$$

The measurement model is defined in (11), which relates the observed measurement z_k to the current state,

$$z_k = Hx_k + v_k \tag{11}$$

For a two-dimensional measurement model, (12) is used.

$$\begin{bmatrix}\theta_k \\ \omega_k\end{bmatrix} = [1 \quad 0]\begin{bmatrix}\theta_{k-1} \\ \omega_{k-1}\end{bmatrix} + \begin{bmatrix}0 \\ 1\end{bmatrix} w_{k-1} \tag{12}$$

where v_k is the measurement noise with zero mean (13) and variance R_v as indicated in (14),

$$\mu_{v_k} = E[v_k] = 0 \tag{13}$$

$$R_v = E[v_k v_k^T] = E[v_k v_j] = \begin{cases} R_v \ , for \ k = j \\ 0 \ , \ for \ k \neq j \end{cases} \tag{14}$$

The expectation operator $E[-]$ signifies the expected value.

The Kalman filter involves two primary stages, Time Update (Prediction) and Measurement Update (Correction) as shown in (5). Process of the kalman filter shown in Fig. 5.

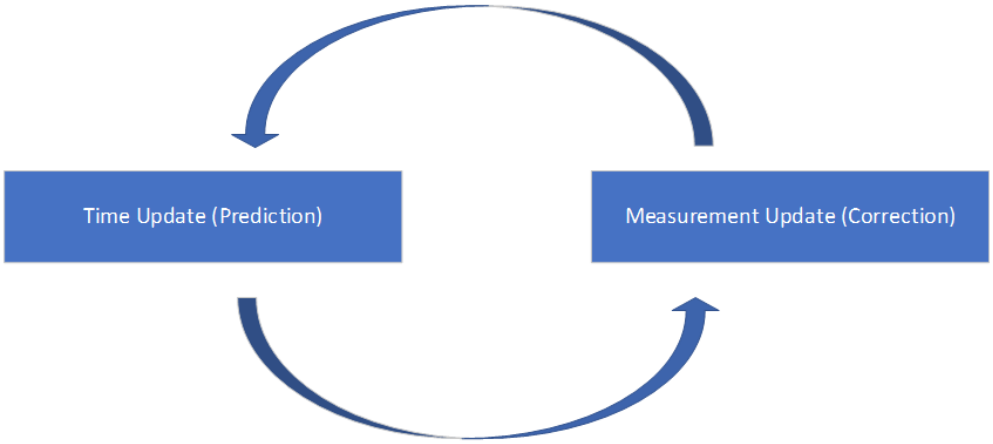

Fig. 5. Process of the kalman filter

The prediction and correction phases are both included in the discrete-time Kalman filter equations.

Time Update (Prediction) Equations

Predicted (a priori) state estimate (15).

$$\hat{x}_k^- = A\hat{x}_{k-1} + Bu_{k-1} \tag{15}$$

Predicted (a priori) estimate covariance (16).

$$P_k^- = AP_{k-1}A^T + BQB^T \tag{16}$$

Measurement Update (Correction) Equations Optimal Kalman gain

Optimal Kalman gain (17).

$$K_k = P_k^- H^T (HP_k^- H^T + R)^{-1} \tag{17}$$

Updated (a posteriori) state estimate (18).

$$\hat{x}_k = \hat{x}_k^- + K_k(z_k - H\hat{x}_k^-) \tag{18}$$

Updated (a posteriori) estimate covariance (19).

$$P_k = (I - K_k H)P_k^- \tag{19}$$

The MPU6050 sensor, which integrates measurements from the accelerometer and gyroscope, utilizes the Kalman filter to process data. Fig. 6 illustrates the standard Kalman filter structure, while

Fig. 7 illustrates an enhanced model. The accelerometer outputs are initially processed through an averaging filter in this enhanced configuration before being inputted into the Kalman filter. This filter is designed to enhance the accuracy of angle estimation by reducing noise and improving data stability.

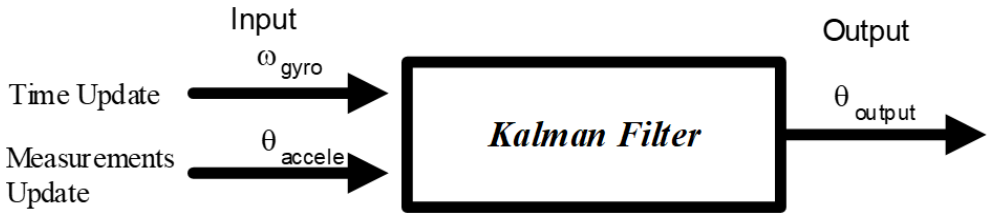

Fig. 6. Block diagram of kalman filter

These are the initialized key parameters for this Kalman filter configuration, $A = 1$, $B = 0.013$, $Q = 1 \times 10^{-12}$,$R = 1 \times 10^{-12}$, $H = 1$, and $I = 1$. The filter is optimized for real-time applications by meticulously selecting these values to achieve a balance between computational efficiency and accuracy.

$$u_k = \omega_{gyro} \tag{20}$$

$$z_k = \theta_{Accele} \tag{21}$$

The estimated angle is represented by the output state variable $\hat{x}_k$ in this system. The angular velocity measured by the gyroscope is denoted by $u_k = \omega_{gyro}$, while the angle obtained from the accelerometer is represented by $z_k = \theta_{Accele}$, as described in (20) and (21). By continuously revising the process and measurement noise covariances, the Kalman filter is intended to manage sensor drift and noise, thereby enabling it to adapt to environmental fluctuations and preserve robustness. This implementation is especially beneficial for applications that necessitate precise angle estimation and stability, such as balance control mechanisms, automotive systems, and robotics.

2.5. Determining Q and R Values in Kalman Filter Implementation

The precise identification of *Q* and *y* values is essential for the efficient implementation of the Kalman filter. The values are obtained from the variance of sensor data, with *Q* indicating the variation of gyroscope readings and *R* denoting the variance of accelerometer readings. This derivation is essential as it allows the filter to enhance its performance by considering both process noise and measurement noise. The input data for the Kalman filter is defined as follows

$$\omega_k = \omega_{gyro} \tag{22}$$

$$\theta_k = \theta_{Accele} \tag{23}$$

At the initial time step *k*=1, *Q* and *R* are set to predefined constant values,

$$Cov(Q) = 1 \times 10^{-12} \tag{24}$$

$$Cov(R) = 1 \times 10^{-12} \tag{25}$$

These initial values are essential for establishing a baseline noise assumption for the Kalman filter.

As the time step progresses, specifically for $k < N$, the values of *Q* and *R* are recalculated using the variance of the available data up to that point. This recalibration is expressed by the following equations,

$$Cov(Q) = \frac{1}{N-1}\sum_{i=1}^{N}(\omega_i - \bar{\omega})^2 \tag{26}$$

$$Cov(R) = \frac{1}{N-1}\sum_{i=1}^{N}(\theta_i - \bar{\theta})^2 \quad (27)$$

When the time step k reaches N, Q and R values are then calculated based on the variance from the most recent N time steps, as shown in the following equations,

$$Cov(Q) = \frac{1}{N-1}\sum_{i=(N-k)}^{k}(\omega_i - \bar{\omega})^2 \quad (28)$$

$$Cov(R) = \frac{1}{N-1}\sum_{i=(N-k)}^{k}(\theta_i - \bar{\theta})^2 \quad (29)$$

```
// Pseudo Code for Determining Q and R Values in Kalman Filter
INITIAL_COVARIANCE = 1e-12
// Initialize Q and R
Q = INITIAL_COVARIANCE
R = INITIAL_COVARIANCE
// Function to calculate variance
function calculate_variance(data, mean, start_index, end_index):
    sum_of_squares = 0
    for i from start_index to end_index:
        sum_of_squares += (data[i] - mean) ^ 2
    return sum_of_squares / (end_index - start_index)
// Function to calculate mean
function calculate_mean(data, start_index, end_index):
    sum = 0
    for i from start_index to end_index:
        sum += data[i]
    return sum / (end_index - start_index + 1)
// Main loop to determine Q and R
for k from 1 to current_time_step:
    if k == 1:
        Q = INITIAL_COVARIANCE
        R = INITIAL_COVARIANCE
    else if k < N:
        mean_gyro = calculate_mean(gyroscope_readings, 1, k)
        mean_accel = calculate_mean(accelerometer_readings, 1, k)
        Q = calculate_variance(gyroscope_readings, mean_gyro, 1, k)
        R = calculate_variance(accelerometer_readings, mean_accel, 1, k)
    else:
        mean_gyro = calculate_mean(gyroscope_readings, k - N + 1, k)
        mean_accel = calculate_mean(accelerometer_readings, k - N + 1, k)
        Q = calculate_variance(gyroscope_readings, mean_gyro, k - N + 1, k)
        R = calculate_variance(accelerometer_readings, mean_accel, k - N + 1, k)
    // Update Kalman filter
    update_kalman_filter(Q, R)
    kalman_predict()
    kalman_update()
```

Fig. 7. Algorithm for estimating Q and R values in kalman filter

This strategy ensures the filter adeptly adjusts to variations in sensor data, which is essential for maintaining optimal performance. The Kalman filter's ability to precisely track and forecast system states in chaotic environments is enhanced by the ongoing adjustment of Q and R. The filter improves state prediction accuracy by dynamically adjusting to varying noise characteristics through recalibration of values using either the complete dataset or recent observations. This versatility is crucial for the precise and reliable filtration of dynamic environments. The pseudocode delineates a thorough approach for ascertaining the values of Q and R. To create a baseline for noise assumptions, Q and R are first assigned a minimal constant value of 1×10^{-12}. The calculate_mean and calculate_variance functions are crucial for ascertaining the mean and variance of designated data ranges, thereby allowing Q and R to adapt constantly to real-time sensor inputs, as seen in Fig. 7.

During each iteration of the primary loop, the filter utilizes the initial constant values for Q and R when $k = 1$. Q and R are recalibrated utilizing all accessible data, adapting to cumulative noise characteristics, as k grows while remaining below N. When k approaches or surpasses N, the most recent N intervals are utilized to update Q and R. This guarantees the system's responsiveness to the latest alterations in sensor data. The ongoing recalibration enables the Kalman filter to adeptly handle varying noise levels, thereby enhancing the accuracy of system state estimates. The Kalman filter enhances angle estimations and guarantees dependable monitoring and prediction of system states, even in turbulent situations, by executing its prediction and correction phases subsequent to the adjustment of Q and R.

3. Results and Discussion

This study evaluates the effectiveness of the Kalman Filter and the Complementary Filter in two distinct environments: high-noise and low-noise conditions. In order to determine the effectiveness of each filter in maintaining reliable outputs under a variety of conditions, the evaluation prioritizes critical performance indicators, including robustness and accuracy. The efficacy of each filtering approach for accurate angle estimation in dynamic systems is critically examined in this comparison research, which elucidates their advantages and disadvantages. The testing procedure was facilitated by the development of a specialized apparatus that captured the angular measurements of the system, as illustrated in Fig. 8. This configuration consisted of a mechanical apparatus that was connected to a 1K adjustable resistor and was intended to accurately measure angles in degrees. The system generated critical angle measurements that were supplied by the MPU6050 sensor, which was connected to the device. The accelerometer was configured to detect forces of up to 4g, while the gyroscope was calibrated for a measurement range of 500 degrees per second. For optimum data logging efficacy, data was captured every 13 milliseconds at a baud rate of 250,000. The algorithm's estimation precision was improved by configuring the Kalman Filter with N set to 20. The experimental findings are detailed in the following sections, and MATLAB was employed to conduct a comprehensive data analysis. The graph titled “Gyroscope” was generated by estimating the angular measurements obtained from the gyroscope using equation (8). Equations (2) and (3) were employed to analyze the accelerometer data for “Accelerometers I” and “Accelerometers II,” respectively. The gyroscope and accelerometer were used to obtain the inputs for the Complementary Filter, which led to the development of “Complementary Filter I.” In the same vein, the inputs used by “Kalman Filter I” were identical. The data from “Accelerometers II” was used to generate the outputs for “Complementary Filter II” and “Kalman Filter II.” This methodical approach enabled a comprehensive assessment of the various filtration methods.

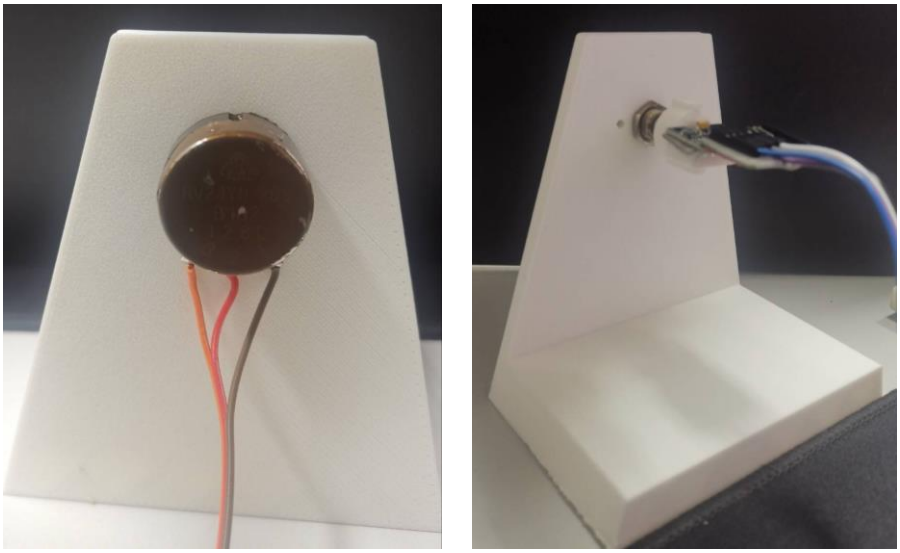

Fig. 8. Mechanical structure for angular measurement

3.1. Evaluation of Angle Measurement Design Under Non-Disturbance Conditions

Using data from the MPU6050 sensor, which provides both accelerometer and gyroscope readings, this work examined how well the Kalman filter and complementary filter approaches for determining angles performed. The experiment was placed in a location free of disturbances; hence, there was no measurement noise. Fig. 9 displays the angle estimates derived from Complementary Filters I, II, and Kalman Filters I and II. With relatively minor variations, the data reveal that every filtering technique got quite near to the real angle. This underlined the accuracy of every technique in low-noise environments. As demonstrated in Fig. 10, the fact that the prediction error for all filters kept inside ±2.5 degrees indicated that these techniques performed effectively in this context. The Q and R numbers, which represent process noise and measurement noise covariance, were adjusted on demand throughout the experiment to provide even better filters. These figures are quite significant as they guide the response of every filter to variations in sensor values. Fig. 7 provides the technique for altering these values. Fig. 10 displays the changes in the Q and R values with time. This guarantees that the filters will perform effectively under the circumstances arising throughout the experiment. The gyroscope data (shown in green in Fig. 11) demonstrated quite minimal variance during the experiment when compared to the Kalman and complementary filters. This implied that it performed effectively in conditions of stability. But the stand-alone gyroscope displayed an inaccuracy that grew with dynamic circumstances added. This is a common issue when angles are estimated using gyroscopes without any other kind of correcting mechanism. Particularly from Accelerometer II, the accelerometer readings displayed considerable fluctuation and a greater error rate. This implies that more precise angle estimations depend on sensor fusion techniques. The Kalman filter demonstrated how robust it was by lowering these errors the greatest while handling both stationary and dynamic circumstances.

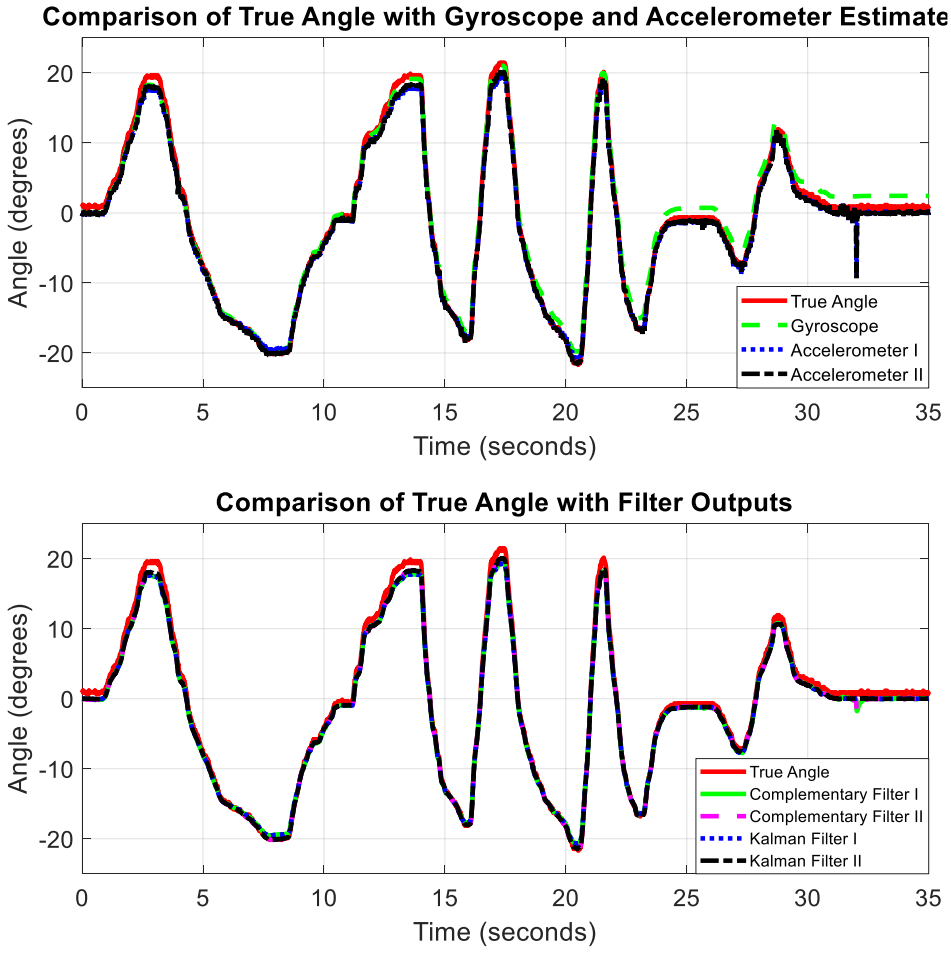

Fig. 9. Angle estimation comparison under non-disturbance conditions

Fig. 9 also offers a thorough comparison of the Kalman filter's and complementary filter's performance. Results from Kalman Filter I and Kalman Filter II were regularly closer to the correct angle than those of their complementary filter equivalents. The gyroscope first produced quite accurate estimates, but as the test went on, the accumulated drift caused more inaccuracy. This phenomenon emphasizes, especially in dynamic contexts, the limits of employing a stationary gyroscope in angle measurement activities.

Fig. 10 show the estimated errors resulting from accelerometer I, accelerometer II, and the gyroscope (red line). Although the gyroscope had quite constant error levels all during the test, with time the cumulative drift became increasingly clear. On the other hand, Accelerometer II's sensitivity to vibrations and quick motions caused noticeably more inaccuracies at designated intervals. Complementary filters and Kalman filters helped lower these mistakes; the Kalman filter routinely shows the lowest total error in all possible cases.

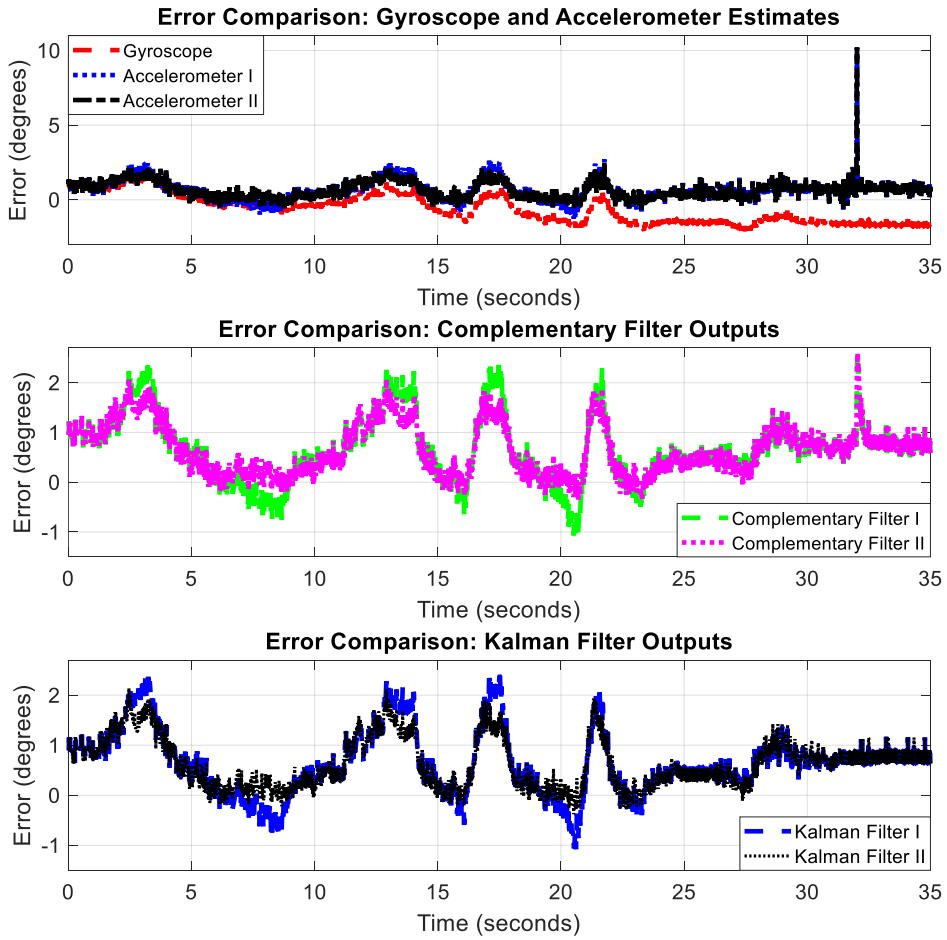

Fig. 10. Error comparison of sensors and filters under non-disturbance conditions

At last, Fig. 11 shows the variances in data gathered from the gyroscope (green), accelerometer I (blue), and accelerometer II (black). Especially at times of fast movement, the gyroscope showed less variance than the accelerometers. Accelerometer I and Accelerometer II both displayed great fluctuation in some areas (e.g., between 10 and 20 seconds), thereby highlighting the instability of applying accelerometer-based readings for precise angle estimation. By reducing these fluctuations, the Kalman filter produced more consistent and steady angle predictions in practical applications, particularly in cases of fast movement or outside disturbance presence.

Finally, the results of this experiment amply show that in terms of angle estimation accuracy, the Kalman filter beats the complementary filter and single sensors. This is especially true in dynamic

surroundings when drift and noise are major issues. Applications include robotics and motion tracking, where exact angle estimation is essential for system performance and benefit from the Kalman Filter's ability to adapt to different noise levels and retain low error rates.

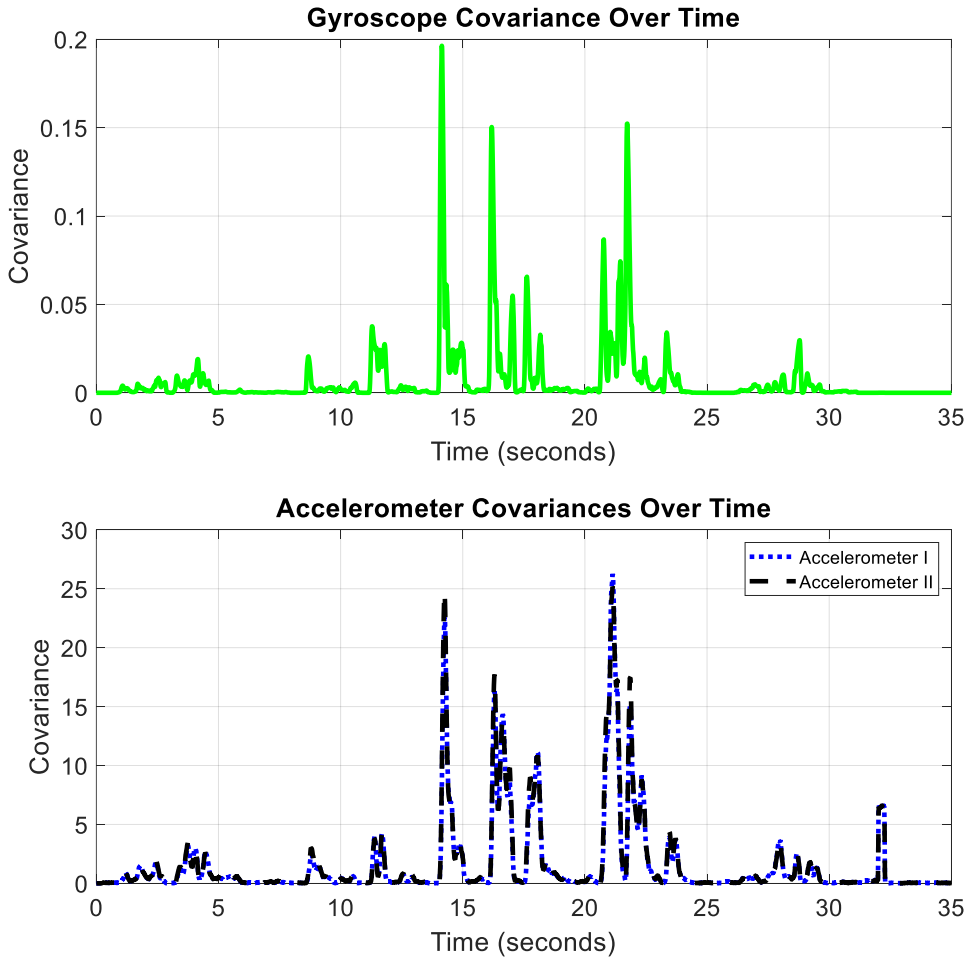

Fig. 11. Covariance of gyroscope and accelerometers under non-disturbance conditions

3.2. Evaluation of Angle Measurement Design Under Disturbance Conditions

Under disturbance conditions, where measurement noise is included in the system, this part of the research assesses the Kalman filter's and complementary filter's performance for angle estimation. The MPU6050 sensor integrated gyroscope and accelerometer measurements gathered the data for this investigation. The aim was to evaluate, under high noise, the accuracy and resilience of every filtering method.

Fig. 12 shows the angular estimations produced by Kalman Filters I and II, Complementary Filters I and II. Although all filters showed variations in noisy conditions, the Kalman filter constantly produced the most accurate estimations, according to the results.

Especially as shown in Fig. 13, the estimate errors for Kalman Filters I and II stayed between ±2.8 and ±2.5 degrees, respectively, thereby verifying their better performance in noisy environments. Dynamic adjustment of values of Q and R, which indicate process and measurement noise covariance, helped to maximize filter performance in high-noise environments.

By showing the changes in these values over time, Fig. 14 enables the Kalman Filter to preserve correct estimations independent of changing noise levels. By comparison, the complementary filters had larger error margins; complementary filter I showed an inaccuracy of ±4.5 degrees, while complementary filter II reached ±13.7 degrees.

Although drift accumulated over time, a typical problem with standalone gyroscopes, particularly in dynamic environments, the gyroscope data (shown in Fig. 12) demonstrated better accuracy than the accelerometer data under disturbance conditions when compared to the Kalman and complementary filters. Particularly Accelerometer II, which showed inaccuracies up to ±153 degrees due to its sensitivity to vibrations and fast motions, Accelerometer I and Accelerometer II showed notably greater error rates. The Kalman Filter's strong ability to control gyroscope drift and accelerometer variation helped to greatly lower these mistakes.

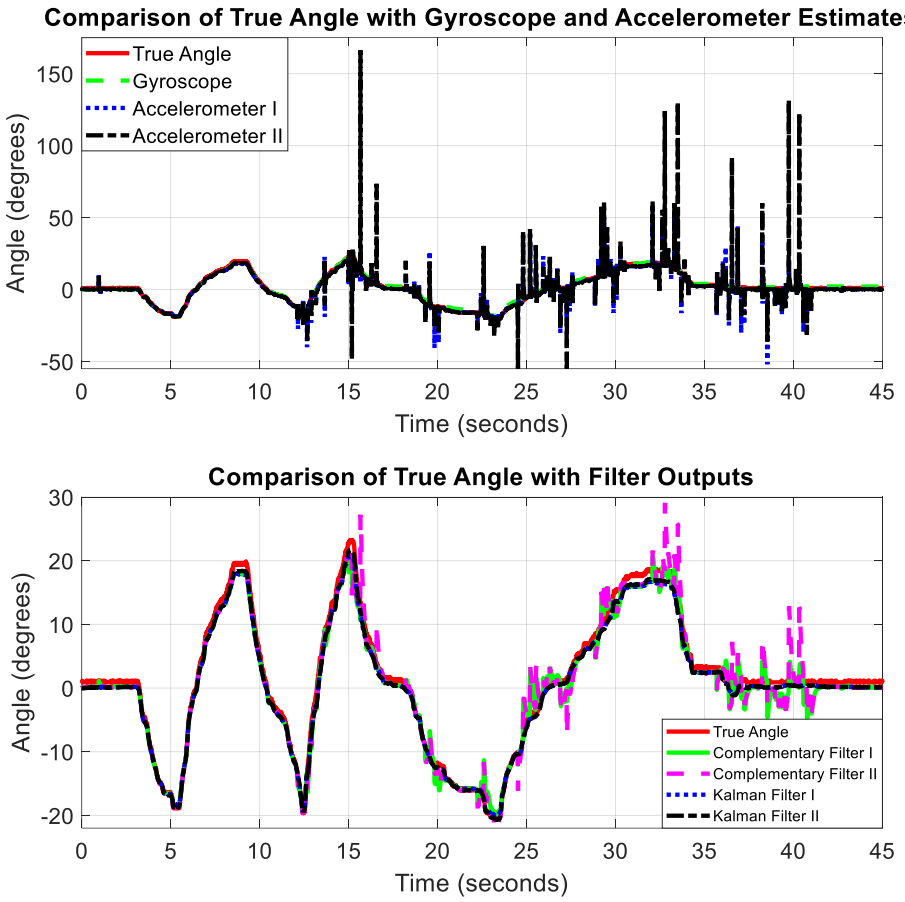

Fig. 12. Angle estimation comparison under disturbance conditions

Fig. 13 also offers a comparison between Kalman filter and complementary filter error margins. With Kalman Filter II performing somewhat better than Kalman Filter I, both filters maintained lower total error rates than the complementary filters. The gyroscope and complementary filters first generated quite precise readings, but when noise levels rose, the complementary filters found it difficult to remain accurate, and so there were notable variations. This emphasizes the restrictions on complementary filters in highly dynamic or high-noise environments.

Fig. 14 shows even more the differences in the gyroscope and accelerometer data collection. The gyroscope showed quite low variation across the trial, suggesting constant functioning even in noisy surroundings. But both Accelerometer I and Accelerometer II showed notable variation, especially in highly disturbed times, that is, between 15 and 25 seconds. More consistent and precise angle estimations made by the Kalman filter helped to minimize these deviations than by the independent sensors.

All things considered, the findings of this experiment amply show that in high-noise environments, the Kalman filter beats the complementary filter and stationary sensors. Although the Kalman Filter was more successful in eliminating cumulative drift and lowering error due to noise and disturbances, the gyroscope gave quite steady performance under noisy settings. Applications

needing an exact angle estimate in contexts where measurement noise is common, including robotics and motion tracking systems, would find the Kalman filter to be the perfect solution as it can dynamically respond to changing noise circumstances.

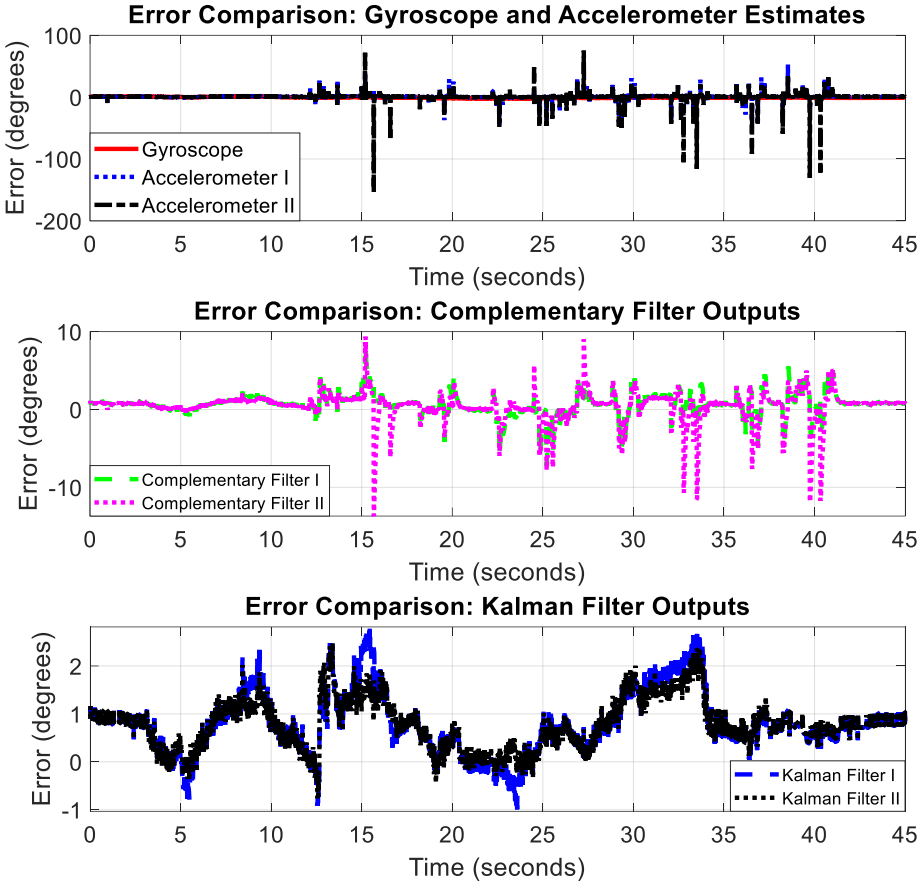

Fig. 13. Error comparison of sensors and filters under disturbance conditions

3.3. Performance Analysis of Filtering Techniques in Low-Noise and Noisy Conditions

With an especially strong emphasis on two important performance indicators, MAE and Root Mean Square Error (RMSE), this portion offers a thorough study of the filters' performance in both low-noise and high-noise environments. Since they represent both the average error and the degree of more significant deviations in estimate results, these signals are crucial for evaluating the accuracy of angle estimation in dynamic systems. Table 1 shows the performance of every filter under low-noise situations based on the results of Section 3.1. Table 2 shows the results for high-noise conditions in Section 3.2. By reducing both the average error and the amplitude of error deviations, Kalman Filter I attained the lowest MAE of 0.6513 and RMSE of 0.8044 in low-noise settings (Table 1), thereby proving its better accuracy in angle estimation. By comparison, the gyroscope filter highlighted its lack of precision without noise mitigation by displaying the greatest MAE (1.0387) and RMSE (1.1940). This suggests that, although offering a baseline approximation, stand-alone sensors such as the gyroscope lack accuracy when compared to filtering methods. Because of the measurement noise introduced in noisy conditions (Table 2), all filters had greater MAE and RMSE values. Particularly the Accelerometer II filter displayed a notable rise with an MAE of 1.7690 and an RMSE of 6.6957, thereby highlighting its great sensitivity to noise. With an MAE of 0.8354 and an RMSE of 1.0055, the Kalman filter maintained quite good performance despite the rising error across all filters. Compared to other filters, this little increase in error emphasizes the Kalman Filter's resilience as it dynamically changes to more successfully manage measurement noise. Especially appropriate for high-noise environments, the rather constant MAE and RMSE figures show the Kalman Filter's capacity to restrict average and severe mistakes.

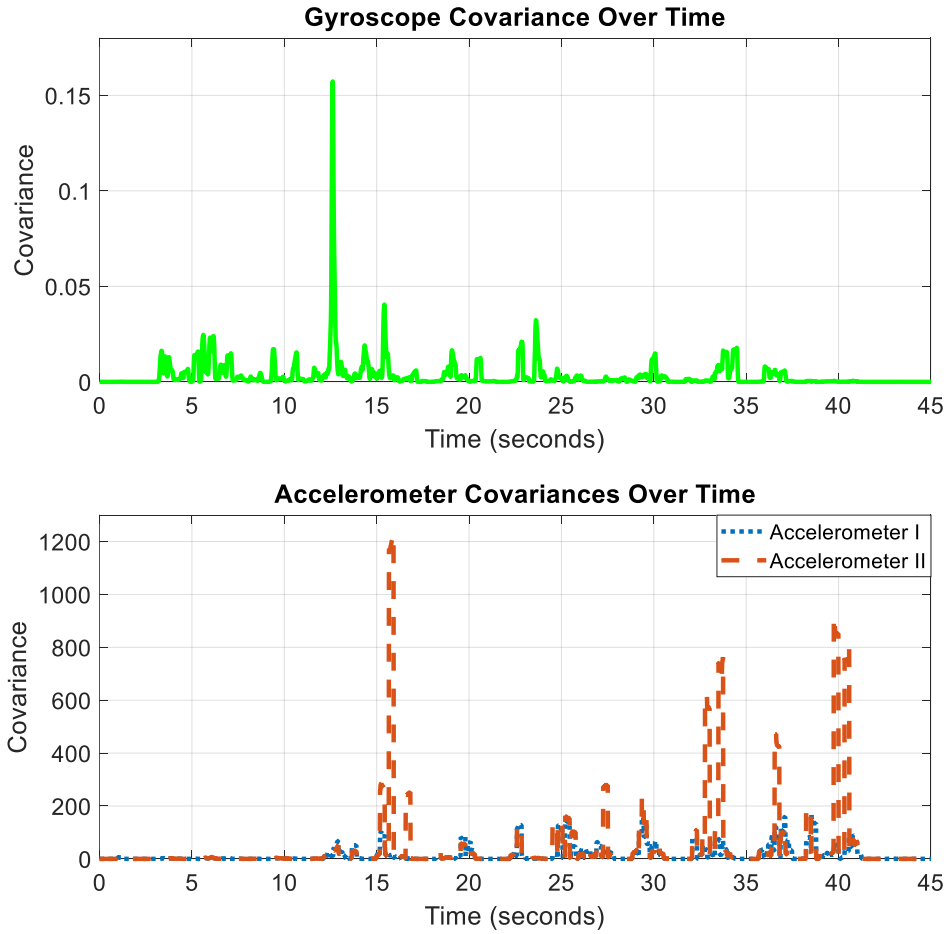

Fig. 14. Covariance of gyroscope and accelerometers under non-disturbance conditions

Table 1. Filter performance in low-noise system

Filter Type	MAE	RMSE
Gyro	1.0387	1.1940
Accelerometer	0.7611	0.9612
Accelerometer II	0.6950	0.8776
Complementary Filter I	0.7463	0.9148
Complementary Filter II	0.6709	0.8256
Kalman Filter	0.7240	0.8913
Kalman Filter I	0.6513	0.8044

Table 2. Filter performance in noise system

Filter Type	MAE	RMSE
Gyro	0.9514	1.1071
Accelerometer	1.5817	4.0350
Accelerometer II	1.7690	6.6957
Complementary Filter I	1.1506	1.5360
Complementary Filter II	1.2568	1.9170
Kalman Filter	0.8354	1.0055
Kalman Filter I	0.7782	0.9156

In terms of MAE and RMSE, the Kalman filter clearly beats other filtering methods when comparing outcomes under both low- and high-noise environments. The complementary filters still have an advantage over stand-alone gyroscope and accelerometer filters, even if their performance suffers when noise is added. This study emphasizes the need for choosing a suitable filter depending

on the working environment. The Kalman Filter's capacity to keep MAE and RMSE values quite low provides a consistent way for dynamic systems experiencing different degrees of noise to retain accuracy.

4. Conclusion

This study examined the Kalman filter and complementary filter for angle estimation with accelerometer and gyroscope data from the IMU6050 sensor. The trials repeatedly demonstrated the Kalman Filter's improved angle estimate precision, particularly in high-noise settings and during rapid movements, while being run under a variety of motion scenarios, including ordinary rotations and scenarios with disturbances and noise. The Kalman filter's durability and adaptability were demonstrated by the lowered mean absolute error and root mean square error measurements. As a result, it is perfect for applications that need precise and consistent angle estimations, such as robotics, motion tracking, and advanced control systems. The dynamic adjustment of Q and R values in the Kalman filter boosts dependability in a variety of conditions and improves responsiveness to variable noise levels, giving it a competitive advantage over static filtering techniques. Furthermore, it enhances reliability. Future research may look at the Kalman Filter's usefulness in complex, real-world settings like autonomous automobiles or wearable technologies, where accuracy and processing efficiency are crucial. This may include an evaluation of its performance across several sensor types. Furthermore, its future applications in biomedical engineering are promising. The Kalman Filter can increase angle measurement accuracy in medical devices such as motor The Kalman Filter helps increase angle measurement accuracy in medical devices, including motorized wheelchairs that balance and lift, telemedicine robots with head-tracking for remote consultations, and adjustable hospital beds. These examples demonstrate the Kalman Filter's effectiveness as a dependable solution in complex systems that require precise control and durable performance in dynamic environments.

Author Contribution: All authors contributed equally to the main contributor to this paper. All authors read and approved the final paper.

Funding: Research Institute, Academic Services Center, and College of Biomedical Engineering, Rangsit University.

Acknowledgment: The researcher would like to thank the Research Institute, Academic Services Center, and College of Biomedical Engineering, Rangsit University for the grant of research funding to the research team. Furthermore, it is confirmed that the project has been reviewed by the Ethics Review Board of Rangsit University, with reference number RSUERB2024-002, which certifies that the research does not involve human subjects.

Conflicts of Interest: The authors declare no conflict of interest.

References

[1] M. Barbary and M. H. A. ElAzeem, “Drones tracking based on robust cubature Kalman-TBD-multi-Bernoulli filter,” *ISA Transactions*, vol. 114, pp. 277-290, 2021, https://doi.org/10.1016/j.isatra.2020.12.042.

[2] K. Ansari and P. Jamjareegulgarn, "Effect of Weighted PDOP on Performance of Linear Kalman Filter for RTK Drone Data," *IEEE Geoscience and Remote Sensing Letters*, vol. 19, pp. 1-4, 2022, https://doi.org/10.1109/LGRS.2022.3204323

[3] M. L. Hoang, M. Carratù, V. Paciello, and A. Pietrosanto, “Fusion Filters between the No Motion No Integration Technique and Kalman Filter in Noise Optimization on a 6DoF Drone for Orientation Tracking,” *Sensors*, vol. 23, no. 12, p. 5603, 2023, https://doi.org/10.3390/s23125603.

[4] E. Lim, "Pose Estimation of a Drone Using Dynamic Extended Kalman Filter Based on a Fuzzy System," *2021 9th International Conference on Control, Mechatronics and Automation (ICCMA)*, pp. 141-145, 2021, https://doi.org/10.1109/ICCMA54375.2021.9646187.

[5] F. J. González-Castaño, F. Gil-Castiñeira, D. Rodríguez-Pereira, J. Á. Regueiro-Janeiro, S. García-Méndez and D. Candal-Ventureira, "Self-Corrective Sensor Fusion for Drone Positioning in Indoor Facilities," *IEEE Access*, vol. 9, pp. 2415-2427, 2021, https://doi.org/10.1109/ACCESS.2020.3048194.

[6] Z. Dai and L. Jing, "Lightweight Extended Kalman Filter for MARG Sensors Attitude Estimation," *IEEE Sensors Journal*, vol. 21, no. 13, pp. 14749-14758, 2021, https://doi.org/10.1109/JSEN.2021.3072887.

[7] F. Marino and G. Guglieri, "Beyond Static Obstacles: Integrating Kalman Filter with Reinforcement Learning for Drone Navigation," *Aerospace*, vol. 11, no. 5, p. 395, 2024, https://doi.org/10.3390/aerospace11050395.

[8] W. An, T. Lin, and P. Zhang, "An Autonomous Soaring for Small Drones Using the Extended Kalman Filter Thermal Updraft Center Prediction Method Based on Ordinary Least Squares," *Drones*, vol. 7, no. 10, p. 603, 2023, https://doi.org/10.3390/drones7100603.

[9] S. Srey and S. Srang, "Adaptive Controller Based on Estimated Parameters for Quadcopter Trajectory Tracking," *International Journal of Robotics and Control Systems*, vol. 4, no. 2, pp. 480-501, 2024, https://doi.org/10.31763/ijrcs.v4i2.1342.

[10] I. Kurniasari and A. Ma'arif, "Implementing PID-Kalman Algorithm to Reduce Noise in DC Motor Rotational Speed Control," *International Journal of Robotics and Control Systems*, vol. 4, no. 2, pp. 958-978, 2024, https://doi.org/10.31763/ijrcs.v4i2.1309.

[11] R. Ikhsan Alfian, A. Ma'arif, and S. Sunardi, "Noise Reduction in the Accelerometer and Gyroscope Sensor with the Kalman Filter Algorithm," *Journal of Robotics and Control (JRC)*, vol. 2, no. 3, pp. 180-189, 2021, https://doi.org/10.18196/jrc.2375.

[12] V. Mansur, S. Reddy, S. R and R. Sujatha, "Deploying Complementary filter to avert gimbal lock in drones using Quaternion angles," *2020 IEEE International Conference on Computing, Power and Communication Technologies (GUCON)*, pp. 751-756, 2020, https://doi.org/10.1109/GUCON48875.2020.9231126.

[13] A. Basiri, V. Mariani, and L. Glielmo, "Improving Visual SLAM by Combining SVO and ORB-SLAM2 with a Complementary Filter to Enhance Indoor Mini-Drone Localization under Varying Conditions," *Drones*, vol. 7, no. 6, p. 404, 2023, https://doi.org/10.3390/drones7060404.

[14] H. Dong, J. Liu, C. Wang, H. Cao, C. Shen and J. Tang, "Drone Detection Method Based on the Time-Frequency Complementary Enhancement Model," *IEEE Transactions on Instrumentation and Measurement*, vol. 72, pp. 1-12, 2023, https://doi.org/10.1109/TIM.2023.3328072.

[15] N. Srinidhi, J. Shreyas, and E. Naresh, "Establishing Self-Healing and Seamless Connectivity among IoT Networks Using Kalman Filter," *Journal of Robotics and Control (JRC)*, vol. 3, no. 5, pp. 646-655, 2022, https://doi.org/10.18196/jrc.v3i5.11622.

[16] B. Skorohod, "Finite Impulse Response Filtering Algorithm with Adaptive Horizon Size Selection and Its Applications," *Journal of Robotics and Control (JRC)*, vol. 3, no. 6, pp. 836-847, 2023, https://doi.org/10.18196/jrc.v3i6.16058.

[17] V. Shenoy and S. Vekata, "Estimation of Liquid Level in a Harsh Environment Using Chaotic Observer," *Journal of Robotics and Control (JRC)*, vol. 3, no. 5, pp. 566-582, 2022, https://doi.org/10.18196/jrc.v3i5.16183.

[18] W. T. Higgins, "A Comparison of Complementary and Kalman Filtering," *IEEE Transactions on Aerospace and Electronic Systems*, vol. AES-11, no. 3, pp. 321-325, 1975, https://doi.org/10.1109/TAES.1975.308081.

[19] P. Vlastos, G. Elkaim and R. Curry, "Low-Cost Validation for Complementary Filter-Based AHRS," *2020 IEEE/ION Position, Location and Navigation Symposium (PLANS)*, pp. 1444-1451, 2020, https://doi.org/10.1109/PLANS46316.2020.9109965.

[20] M. Al Borno *et al*., "OpenSense: An open-source toolbox for inertial-measurement-unit-based measurement of lower extremity kinematics over long durations," *Journal of Neuroengineering and Rehabilitation*, vol. 19, no. 1, p. 22, 2022, https://doi.org/10.1186/s12984-022-01001-x.

[21] R. V. Vitali, R. S. McGinnis and N. C. Perkins, "Robust Error-State Kalman Filter for Estimating IMU Orientation," *IEEE Sensors Journal*, vol. 21, no. 3, pp. 3561-3569, 2021, https://doi.org/10.1109/JSEN.2020.3026895.

[22] M. Khodarahmi and V. Maihami, "A review on Kalman filter models," *Archives of Computational Methods in Engineering*, vol. 30, no. 1, pp. 727-747, 2023, https://doi.org/10.1007/s11831-022-09815-7.

[23] J. Khodaparast, "A Review of Dynamic Phasor Estimation by Non-Linear Kalman Filters," *IEEE Access*, vol. 10, pp. 11090-11109, 2022, https://doi.org/10.1109/ACCESS.2022.3146732.

[24] A. K. Singh, "Major development under Gaussian filtering since unscented Kalman filter," *IEEE/CAA Journal of Automatica Sinica*, vol. 7, no. 5, pp. 1308-1325, 2020, https://doi.org/10.1109/JAS.2020.1003303.

[25] H. Liu, F. Hu, J. Su, X. Wei and R. Qin, "Comparisons on Kalman-Filter-Based Dynamic State Estimation Algorithms of Power Systems," *IEEE Access*, vol. 8, pp. 51035-51043, 2020, https://doi.org/10.1109/ACCESS.2020.2979735.

[26] R. Hartley, M. Ghaffari, R. M. Eustice, and J. W. Grizzle, "Contact-aided invariant extended Kalman filtering for robot state estimation," *The International Journal of Robotics Research*, vol. 39, no. 4, pp. 402-430, 2020, https://doi.org/10.1177/0278364919894385.

[27] Y. T. Bai, X. Y. Wang, X. B. Jin, Z. Y. Zhao, and B. H. Zhang, "A neuron-based kalman filter with nonlinear autoregressive model," *Sensors*, vol. 20, no. 1, p. 299, 2020, https://doi.org/10.3390/s20010299.

[28] I. Ullah, X. Su, X. Zhang, and D. Choi, "Simultaneous localization and mapping based on Kalman filter and extended Kalman filter," *Wireless Communications and Mobile Computing*, vol. 2020, p. 2138643, 2020, https://doi.org/10.1155/2020/2138643.

[29] P. Poncela, E. Ruiz, and K. Miranda, "Factor extraction using Kalman filter and smoothing: This is not just another survey," *International Journal of Forecasting*, vol. 37, no. 4, pp. 1399-1425, 2021, https://doi.org/10.1016/j.ijforecast.2021.01.027.

[30] Y. Huang, Y. Zhang, Y. Zhao, P. Shi and J. A. Chambers, "A Novel Outlier-Robust Kalman Filtering Framework Based on Statistical Similarity Measure," *IEEE Transactions on Automatic Control*, vol. 66, no. 6, pp. 2677-2692, 2021, https://doi.org/10.1109/TAC.2020.3011443.

[31] M. Impraimakis and A. W. Smyth, "An unscented Kalman filter method for real-time input-parameter-state estimation," *Mechanical Systems and Signal Processing*, vol. 162, p. 108026, 2022, https://doi.org/10.1016/j.ymssp.2021.108026.

[32] S. Sharma, A. Majumdar, V. Elvira and É. Chouzenoux, "Blind Kalman Filtering for Short-Term Load Forecasting," *IEEE Transactions on Power Systems*, vol. 35, no. 6, pp. 4916-4919, 2020, https://doi.org/10.1109/TPWRS.2020.3018623.

[33] Y. Huang, F. Zhu, G. Jia and Y. Zhang, "A Slide Window Variational Adaptive Kalman Filter," *IEEE Transactions on Circuits and Systems II: Express Briefs*, vol. 67, no. 12, pp. 3552-3556, 2020, https://doi.org/10.1109/TCSII.2020.2995714.

[34] E. R. Potokar, K. Norman and J. G. Mangelson, "Invariant Extended Kalman Filtering for Underwater Navigation," *IEEE Robotics and Automation Letters*, vol. 6, no. 3, pp. 5792-5799, 2021, https://doi.org/10.1109/LRA.2021.3085167.

[35] W. Wen, T. Pfeifer, X. Bai, and L. T. Hsu, "Factor graph optimization for GNSS/INS integration: A comparison with the extended Kalman filter," *NAVIGATION: Journal of the Institute of Navigation*, vol. 68, no. 2, pp. 315-331, 2021, https://doi.org/10.1002/navi.421.

[36] K. D. T. Rocha and M. H. Terra, "Robust Kalman filter for systems subject to parametric uncertainties," *Systems & Control Letters*, vol. 157, p. 105034, 2021, https://doi.org/10.1016/j.sysconle.2021.105034.

[37] M. Song, R. Astroza, H. Ebrahimian, B. Moaveni, and C. Papadimitriou, “Adaptive Kalman filters for nonlinear finite element model updating,” *Mechanical Systems and Signal Processing*, vol. 143, p. 106837, 2020, https://doi.org/10.1016/j.ymssp.2020.106837.

[38] H. Fang, M. A. Haile and Y. Wang, "Robust Extended Kalman Filtering for Systems With Measurement Outliers," *IEEE Transactions on Control Systems Technology*, vol. 30, no. 2, pp. 795-802, 2022, https://doi.org/10.1109/TCST.2021.3077535.

[39] G. Hu, B. Gao, Y. Zhong, and C. Gu, “Unscented Kalman filter with process noise covariance estimation for vehicular INS/GPS integration system,” *Information Fusion*, vol. 64, pp. 194-204, 2020, https://doi.org/10.1016/j.inffus.2020.08.005.

[40] W. Wang, N. He, K. Yao, and J. Tong, “Improved Kalman filter and its application in initial alignment,” *Optik*, vol. 226, p. 165747, 2021, https://doi.org/10.1016/j.ijleo.2020.165747.

[41] A. Tsiamis and G. J. Pappas, "Online Learning of the Kalman Filter With Logarithmic Regret," *IEEE Transactions on Automatic Control*, vol. 68, no. 5, pp. 2774-2789, 2023, https://doi.org/10.1109/TAC.2022.3207670.

[42] Y. Sun, W. Bao, K. Valk, C. C. Brauer, J. Sumihar, A. H. Weerts, “Improving forecast skill of lowland hydrological models using ensemble Kalman filter and unscented Kalman filter,” *Water Resources Research*, vol. 56, no. 8, p. e2020WR027468, 2020, https://doi.org/10.1029/2020WR027468.

[43] Y. Huang, G. Jia, B. Chen and Y. Zhang, "A New Robust Kalman Filter With Adaptive Estimate of Time-Varying Measurement Bias," *IEEE Signal Processing Letters*, vol. 27, pp. 700-704, 2020, https://doi.org/10.1109/LSP.2020.2983552.

[44] S. Yi and M. Zorzi, "Robust Kalman Filtering Under Model Uncertainty: The Case of Degenerate Densities," *IEEE Transactions on Automatic Control*, vol. 67, no. 7, pp. 3458-3471, 2022, https://doi.org/10.1109/TAC.2021.3106861.

[45] M. Bai, Y. Huang, B. Chen and Y. Zhang, "A Novel Robust Kalman Filtering Framework Based on Normal-Skew Mixture Distribution," *IEEE Transactions on Systems, Man, and Cybernetics: Systems*, vol. 52, no. 11, pp. 6789-6805, 2022, https://doi.org/10.1109/TSMC.2021.3098299.

[46] A. Hasan, "eXogenous Kalman Filter for State Estimation in Autonomous Ball Balancing Robots," *2020 IEEE/ASME International Conference on Advanced Intelligent Mechatronics (AIM)*, pp. 1522-1527, 2020, https://doi.org/10.1109/AIM43001.2020.9158896.

[47] Y. Cheng, Y. Li, K. Li, X. Liu, C. Liu, X. Hao, “Fusing LSTM neural network and expanded disturbance Kalman filter for estimating external disturbing forces of ball screw drives,” *Robotics and Computer-Integrated Manufacturing*, vol. 89, p. 102776, 2024, https://doi.org/10.1016/j.rcim.2024.102776.

[48] Y. Kang, Z. Qiu, X. Huang, Z. Kong, F. Gu, A. D. Ball, “Field simultaneous estimation of residual unbalance and bearing dynamic coefficients for double-disk rotor-bearing system using dual augmented Kalman filter,” *Journal of Sound and Vibration*, vol. 577, p. 118325, 2024, https://doi.org/10.1016/j.jsv.2024.118325.

[49] A. Srichandan, J. Dhingra, and M. K. Hota, “An improved Q-learning approach with Kalman filter for self-balancing robot using OpenAI,” *Journal of Control, Automation and Electrical Systems*, vol. 32, no. 6, pp. 1521-1530, 2021, https://doi.org/10.1007/s40313-021-00786-x.

[50] R. Dian Alarmi, A. Husein Alasiry, N. Fajar Satria and B. Sumantri, "A Sensor Fusion Algorithm in Humanoid Robot PD Balancing Control for Walking on Slope," *2020 International Electronics Symposium (IES)*, pp. 289-296, 2020, https://doi.org/10.1109/IES50839.2020.9231674.

[51] J. Zhao, J. Li, and J. Zhou, “Research on two-round self-balancing robot SLAM based on the gmapping algorithm,” *Sensors*, vol. 23, no. 5, p. 2489, 2023, https://doi.org/10.3390/s23052489.

[52] W. Youn and S. Andrew Gadsden, "Combined Quaternion-Based Error State Kalman Filtering and Smooth Variable Structure Filtering for Robust Attitude Estimation," *IEEE Access*, vol. 7, pp. 148989-149004, 2019, https://doi.org/10.1109/ACCESS.2019.2946609.

[53] H. A. O. Mohamed *et al*., "Momentum-Based Extended Kalman Filter for Thrust Estimation on Flying Multibody Robots," *IEEE Robotics and Automation Letters*, vol. 7, no. 1, pp. 526-533, 2022, https://doi.org/10.1109/LRA.2021.3129258.

[54] P. Chotikunnan and B. Panomruttanarug, “The application of fuzzy logic control to balance a wheelchair,” *Journal of Control Engineering and Applied Informatics*, vol. 18, no. 3, pp. 41-51, 2016, http://www.ceai.srait.ro/index.php?journal=ceai&page=article&op=view&path%5B%5D=3173.

[55] C. Urrea and R. Agramonte, “Kalman filter: historical overview and review of its use in robotics 60 years after its creation,” *Journal of Sensors*, vol. 2021, p. 9674015, 2021, https://doi.org/10.1155/2021/9674015.

[56] L. Mei *et al*., “Realtime mobile bandwidth prediction using LSTM neural network and Bayesian fusion,” *Computer Networks*, vol. 182, p. 107515, 2020, https://doi.org/10.1016/j.comnet.2020.107515.

[57] S. O. H. Madgwick, S. Wilson, R. Turk, J. Burridge, C. Kapatos and R. Vaidyanathan, "An Extended Complementary Filter for Full-Body MARG Orientation Estimation," *IEEE/ASME Transactions on Mechatronics*, vol. 25, no. 4, pp. 2054-2064, 2020, https://doi.org/10.1109/TMECH.2020.2992296.